Pendulum Beams: Optical Modes that Simulate the Quantum Pendulum

E.J. Galvez, F.J. Auccapuclla, Y. Qin, K.L. Wittler, and J.M. Freedman

Department of Physics and Astronomy, Colgate University, Hamilton, NY 13346, U.S.A.

E-mail: `egalvez@colgate.edu`

1 February 2021

Abstract. The wave equation of electromagnetism, the Helmholtz equation, has the same form as the Schrödinger equation, and so optical waves can be used to study quantum mechanical problems. The electromagnetic wave solutions for non-diffracting beams lead to the 2-dimensional Helmholtz equation. When expressed in elliptical coordinates the solution of the angular part is the same as the Schrödinger equation for the simple pendulum. The resulting optical eigenmodes, Mathieu modes, have an optical Fourier transform with a spatial intensity distribution that is proportional to the quantum mechanical probability for the pendulum. Comparison of Fourier intensities of eigenmodes are in excellent agreement with calculated quantum mechanical probabilities of pendulum stationary states. We further investigate wave-packet superpositions of a few modes and show that they mimic the libration and the nonlinear rotation of the classical pendulum, including revivals due to the quantized nature of superpositions. The ability to "dial a wavefunction" with the optical modes allows the exploration of important aspects of quantum wave-mechanics and the pendulum that may not be possible with other physical systems.

Keywords: Pendulum beams, Mathieu beams, Non-diffracting beams, Quantum pendulum.

1. Introduction

The physical world contains many systems that involve distinct phenomena and parameter scales but which share the same mathematical description. In the case of electromagnetic-wave propagation, the Helmholtz wave equation has similarities with the Schrödinger equation. The former, derived from the general electromagnetic wave equation after assuming that the solution has a harmonic dependence, yields a differential equation that depends only on spatial coordinates, which has the same form as the time-independent Schrödinger equation. This parallel between light and a quantum physical system can be exploited for learning about the quantum system by analogy [1]. The particular system that we consider in this study is the simple pendulum.

The quantum solution of the pendulum was first obtained by Condon in 1928 [2]. His treatment reduced the Schrd̈inger equation to the Mathieu equation [3]. Because of the weakness of gravity relative to electric forces, microscopic pendula are not possible. However, a number of systems show pendulum-like features, such as molecules in the presence of static electric fields [4, 5]. The advent of modern techniques to manipulate fields and materials has led to systems that have a potential with the same cosine dependence as the unperturbed pendulum, such as atoms in the magneto-optical trap [6], anharmonic oscillations in Bose-Einstein condensates [7], and the transmon oscillator in the Josephson-junction superconducting qubit [8]. A periodically driven pendulum or rotor has also been a model system for the study of quantum chaos [9, 10] with laboratory recreations in the the motion of atoms in an optical lattice [11].

When the solution of the 3-d Helnholtz equation is decomposed into a function of the transverse coordinates in conjunction with a longitudinal plane wave, the equation reduces to the 2-d Helmholtz equation. The resulting beams are known as non-diffracting, because over a spatial range they maintain shape and size. Bessel beams were the first type of non-diffracting beams to be studied [12, 13], obtained when the transverse mode is restricted to be angularly uniform. When the transverse component is allowed to have 2-d symmetries, other non-diffracting beams are possible, such as Mathieu beams (connected to the present work) [14, 15], parabolic beams [16, 17], Airy beams [18, 19], and Pearcey beams [20]. All of these these beams have unique propagation properties and contain optical singularities [21].

When the transverse coordinates are transformed into elliptical coordinates, separation of variables leads to radial and angular Mathieu equations [14], with the latter being identical to the quantum pendulum equation. More remarkable is that the far-field pattern of the beam, or equivalently the optical Fourier transform of the mode, performed by a lens, reduces to a ring (owing to the radial solutions expressed in terms of Bessel functions) modulated by the absolute-value square of the angular solution. This modulation has an exact correspondence to the quantum mechanical probability for finding the pendulum as a function of the angular coordinate [22]. In this article we investigate the modes that result from these solutions and compare the light patterns to quantum probabilities. We explore stationary states, wavepacket superpositions and other aspects of the quantum problem.

The article is organized as follows. In Sec. 2 we begin by presenting the theory in two subsections: on the pendulum in Sec. 2.1, and on the quantum pendulum modes in Sec. 2.2. It is followed by a description of the apparatus in Sec. 3. Our experimental results are divided into stationary states, in Sec. 4.1, and wavepacket superpositions in Sec 4.2. We give concluding remarks in Sec. 5.

2. Theoretical Background

2.1. The Quantum Pendulum

The rigid pendulum of length l and mass m is shown in Fig. 1(a). The potential energy

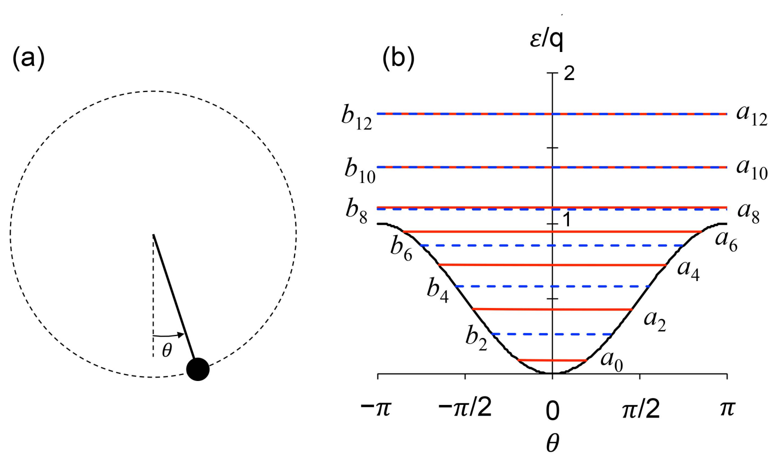

Figure 1. (a) Schematic of the pendulum. (b) Energy level diagram for the case $q = 30$, showing also the cosine-shaped potential barrier. The even(odd) levels are denoted by solid(dashed) horizontal lines.

is given by:

$$V = mgl\,(1 - \cos\theta)\,, \tag{1}$$

with g being the acceleration of gravity. The complete classical solution of this problem leads to interesting nonlinear dynamics [23]. The quantization of this problem leads to the Mathieu equation [5]

$$\frac{d^2\psi}{d\chi^2} + (a - 2q\cos 2\chi)\psi = 0, \tag{2}$$

where a is the energy eigenvalue. The constant $q = 2mgl/E_0$ is a dimensionless parameter representing the scaled height of the potential energy barrier, with $E_0 = \hbar^2/2ml^2$. If m were the mass of the electron and l the atomic radius, this scaling unit is the familiar Bohr energy, $E_0 = 13.6$ eV. An alternative quantum/classical explanation for q is: $\sqrt{q}$ is the ratio of l to the reduced de Broglie wavelength [24]. Thus, we should understand that low values of q refer to situations where quantum mechanics is the appropriate description, and when $q \to \infty$ we reach the classical limit. The variable χ relates to the pendulum angle by

$$\theta = 2\chi. \tag{3}$$

The scaled energy is [5]:

$$\varepsilon = \frac{a}{4} + \frac{q}{2} \tag{4}$$

The eigenvalues of Eq. 2 are divided into two groups corresponding to the cosine-like and sine-like solutions, of respective even and odd symmetry. It is traditional to label the even and odd eigenvalues by a_n and b_n, where n is the quantum number (n is a positive even integer, with $n = 0$ allowed only for the even solution) [3].

Figure 1(b) shows the energy-level diagram for the particular value $q = 30$, which adjusts well to our experimental conditions. We can relate the energy states to salient elements of the classical system: turning-point angle $\theta_{\rm tp}$ for energies below the barrier; and above the barrier, the ratio of instantaneous angular frequencies when the pendulum bob is at the top and bottom of the trajectory, $\omega_{\rm top}/\omega_{\rm bot}$. Table 1 gives the values of these quantities for the energy levels shown in Fig. 1(b).

The wavefunctions are given in terms of their parity, but are not expressed in a closed form:

$$\mathrm{ce}_n(\chi; q) = \sum_{k=0}^{\infty} A_k \cos(k\chi) \qquad n = 0, 2, 4, \ldots \tag{5}$$

$$\mathrm{se}_n(\chi; q) = \sum_{k=2}^{\infty} B_k \sin(k\chi) \qquad n = 2, 4, 6, \ldots \tag{6}$$

where k is an even integer. $\mathrm{ce}_n(\chi; q)$ and $\mathrm{se}_n(\chi; q)$ are the cosine-elliptical and sine-elliptical Mathieu functions, respectively; and A_k and B_k are coefficients that result from the solution [25].

In Figs. 2(a), 2(e) and 2(i) we show the calculated quantum mechanical probability of finding the pendulum at an angle θ in the interval $[-\pi, \pi]$ for states with $n = 4$, $n = 6$ and $n = 10$, respectively. They show salient aspects of the quantization of this mechanical system. The first two states have even symmetry and energies below the barrier, as listed in Table 1. The latter shows evidence of tunneling through the barrier by the continuous non-zero probability in the classically forbidden regions, at angles above the turning points. The state with $n = 10$ is above the barrier, corresponding to a classical rotor that goes faster at the bottom than at the top, yet it has zero probability of being in the inverted position ($\theta = -\pi, \pi$) due to the odd symmetry of the quantum wavefunction.

Table 1. Classical parameters of the pendulum with energies corresponding to low-lying states of the quantum pendulum for $q = 30$. Values include states of even and odd symmetry, except for the ground state, which only has even symmetry.

n	ε/q even(odd)	$\theta_{\rm tp}$ (deg) even(odd)	$\omega_{\rm top}/\omega_{\rm bot}$ even(odd)
0	0.09	35	
2	0.43(0.26)	82(62)	
4	0.72(0.58)	116(99)	
6	0.94(0.85)	152(135)	
8	1.10(1.09)		0.31(0.29)
10	1.37(1.37)		0.52(0.52)
12	1.73(1.73)		0.65(0.65)

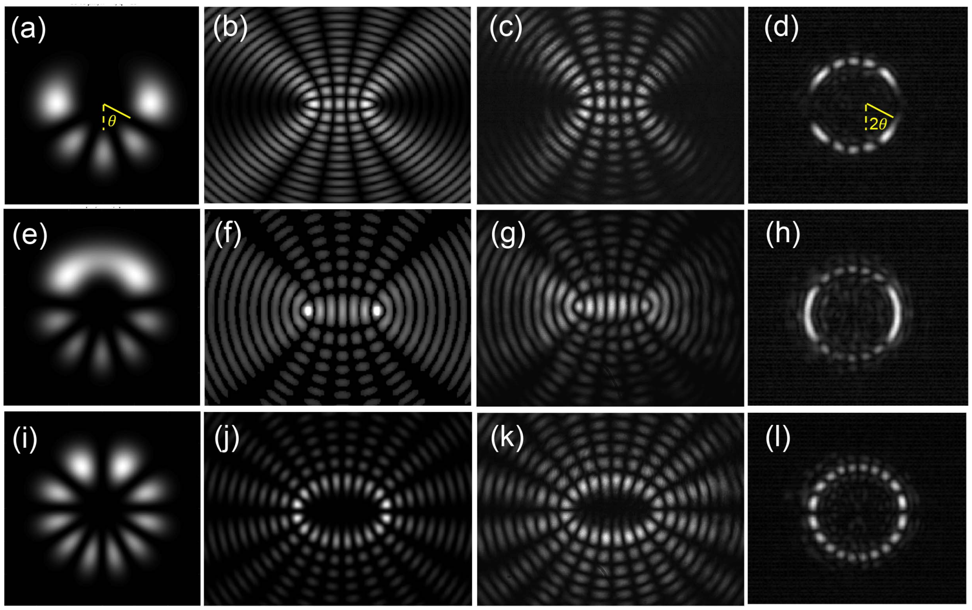

Figure 2. Images corresponding stationary states with $n = 4$ (a-d), $n = 6$ (e-h) and $n = 10$ (i-l) in the following categories: theoretical calculations of the pendulum probability in (a), (e), (i); calculated optical modes in (b), (f), (j), measured modes in (c), (g), (k); and measured Fourier transform patterns in (d), (h) and (l).

2.2. Pendulum Beams

Separation of variables of the 2-d Helmholtz equation in elliptic-radial (ξ) and elliptical-angular (χ) coordinates leads to radial and angular Mathieu equations [14]. The n-th order eigenmodes of even and odd parity are given respectively by

$$U_e(\xi, \chi) = \mathrm{ce}_n(\chi; q)\mathrm{Je}_n(\xi; q) \tag{7}$$

and

$$U_o(\xi, \chi) = \mathrm{se}_n(\chi; q)\mathrm{Jo}_n(\xi; q), \tag{8}$$

where $\mathrm{Je}_n(\xi; q)$ and $\mathrm{Jo}_n(\xi; q)$ are the radial Mathieu functions of even and odd symmetry, respectively [25]. Combination of the two parity solutions of the same order but 90 degrees out of phase gives rise to the helical Mathieu beams, which carry orbital angular momentum and contain n optical vortices in a linear arrangement [26]. In Fig. 2 (b), (f) and (j) we show theoretical modelings of the intensity patterns of the modes with $n = 4, 6, 10$ discussed above for $q = 30$. Note that they have hyperbolic angular and elliptical radial nodes. The number of angular nodes corresponds to n for even states and to $n + 1$ for the odd states.

Because the radial Mathieu functions can be expressed in terms of Bessel functions, the optical Fourier transform gives

$$\mathrm{FT}[U_e(\xi, \chi; q)] = \mathrm{ce}_n(\theta/2; q)\delta(k - k_t) \tag{9}$$

$$\mathrm{FT}[U_o(\xi, \chi; q)] = \mathrm{se}_n(\theta/2; q)\delta(k - k_t), \tag{10}$$

where δ is the Dirac delta function. Notice that this is basically a ring at a radius k_t modulated by the angular solution. Thus the intensity pattern along the ring is proportional to the quantum mechanical probability. Because of Eq. 3 the quantum probability has a 1:2 mapping to the ring in the Fourier plane.

3. Apparatus

We generated pendulum beams using the optical arrangement shown schematically in Fig. 3. The light from a helium-neon laser was expanded, spatially filtered and collimated before being sent to an SLM (Hamamatsu model LCOS-X10468-07). We encoded the SLM with a combination of phase and amplitude modulation, shown in the insert of Fig. 3, so that the desired mode was generated in the first diffractive order. Both the phase and amplitude modulations contained the Mathieu function information, generated by numerical calculations using a Matlab computational toolbox [27]. A pair of lenses re-imaged the beam using a 4-f configuration. In between, at the Fourier plane of the SLM, an adjustable iris spatially filtered the desired mode, eliminating light from undesired diffracted orders. Past the second lens the non-diffracting pendulum beam was formed over a range of 50 cm. A beam splitter deflected part of the beam to a lens for recording the image in the Fourier plane of the mode. Two digital cameras (Thorlabs model DCC1545M) were used to record the mode and its Fourier transform.

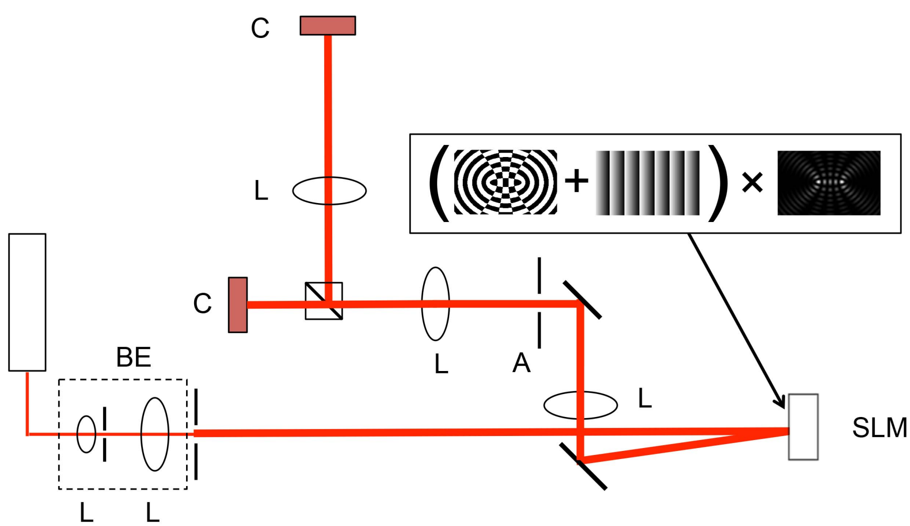

Figure 3. Schematic of the apparatus. Optical components include laser, beam expander (BE), lenses (L), apertures (A), a spatial light modulator (SLM) and cameras (C). Insert shows an example of the programming of the SLM.

4. Measurements

4.1. Stationary States

We prepared pendulum modes as described in the next section, and imaged the beam modes and their optical Fourier transform. Images (c), (g) (k) in Fig. 2 show the measured modes corresponding to the states $n = 4, 6, 10$, respectively. It can be seen that they reproduce the expectations in panes (b), (f) and (j), respectively. In panes (d), (h) and (l) we show the corresponding imaged Fourier transforms. The observed pattern has a 2:1 correspondence with the actual probability due to Eq. 3. To verify this we integrated the camera pixels along the ring as a function of angle, normalized them and graphed them with the calculated quantum mechanical probability. A comparison for the three cases of Fig. 2 is given in Fig. 4. To avoid confusion we show only the comparison with the bottom half of the measured optical Fourier transform, given that top and bottom halves contain the same information. The agreement between the data and theory is remarkable, especially on the relative location of the minima and maxima and the relative height of the maxima. The only adjustable parameter was the location of $\theta = 0$ between of the data and theory; a correction of about 1 degree due to a slight angular misalignment between the encoding and decoding electronic imaging systems. The only places where there is ambiguity is at $\theta = \pi$, due to contamination of diffractive orders produced by the mode encoding device (SLM). We have also added the calculated classical probabilities (dashed lines), which for the oscillating states rise sharply at the turning points.

4.2. Wavepacket Superpositions

Another interesting case that can be investigated is the inverted pendulum, which has been subject of previous discussions [24]. In principle, if the bob gets an initial energy exactly equal to the barrier height, the pendulum will slow down as it goes up, taking an infinite amount of time to reach the top at which point it will remain at rest. Of course, such a situation is not physically realizable because it would require us to know the position and momentum of the bob with absolute precision, violating the Heisenberg uncertainty principle. Yet, it can be used to study how close to physically realizable situations one can get using wavepacket superpositions.

Since we can program any mode that we desire, we can also program superpositions of modes. Ideally, a Gaussian superposition would mimic the classical pendulum. In practical terms, there is an upper-limit for q in our experiments because the spacing between the zeros along the radial-elliptic coordinate decreases as q increases. This collides with the resolution of our SLM. Thus, for our current experimental values, $q = 30 - 80$ is a reasonable range for high-resolution studies.

To create a wavepacket that mimics the classical pendulum system we create a superpoposition of states (modes) with relative phases that mimic the quantum time evolution for the time-independent Hamiltonian. Thus, we programmed the phase

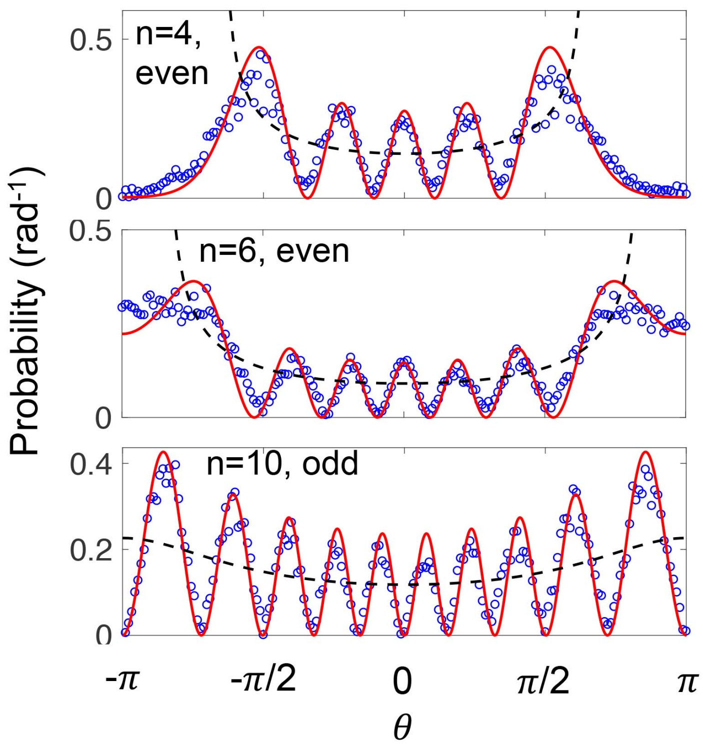

Figure 4. Plot of the normalized light intensity measured at the optical Fourier transform plane (symbols), the calculated quantum mechanical probability (solid line), and classical probabilities (dashed lines); for the 3 states of Fig. 2 with $n = 4, 6, 10$.

associated to each state (mode) to be proportional to the energy of the state. We have investigated a number of cases in this situation.

Consider the superposition of 4 states for the case where the scaled barrier height is $q = 30$:

$$U(t) = a u_{n,e} e^{-i\varepsilon_{n,e}\tau} + b u_{n,o} e^{-i\varepsilon_{n,o}\tau} + c u_{n-2,e} e^{-i\varepsilon_{n-2,e}\tau} + d u_{n-2,o} e^{-i\varepsilon_{n-2,o}\tau}, \quad (11)$$

where a, b, c, d are constants, n stands for a quantum number denoting the state, e and o denoting the parity of the state (even or odd, respectively), $\varepsilon_i = E_i/E_0$ representing the scaled energy of state i, and $\tau = t/(\hbar/E_0)$ scaled time with $\hbar$ being the reduced Planck constant. We created two types of superpositions expressed by Eq. 11: for states below the barrier, with $n = 6$, and for states above the barrier with $n = 10$. The energy level diagram of these two sets of states is shown in Fig. 1(b).

With only 4 states we get modes that already mimic the classical pendulum to a large degree. Figure 5 shows a sequence of modes created with the superposition of Eq. 11 with $n = 6$ and $a = c = 1/2$ and $b = d = +i/2$. At $\tau = 0.5$ we get a snake-looking mode corresponding to the quantum state of the superposition at the left turning point, as shown in Fig. 5(a). We note that the non-diffracting character of the beam was quite evident in the laboratory, as the shape and size of the mode remained unchanged by about 50 cm.

In Fig. 5(b) we show the measured intensity of the corresponding optical Fourier transform, extracted similarly to the data of Fig. 4. It is shown in a polar-type plot, graphed as a function of the real angle of the pendulum, similar to the theoretical modelings of stationary states in Figs. 2(a,e,i). The measured intensity shows that the quantum probability is concentrated at an angle of about $123 \pm 35°$ (centroid with half-width at half maximum), which is consistent with the classical turning points of the $n = 4$ and $n = 6$ states shown in Table 1. We have also done separate modelings of this situation, which agree with the measurements.

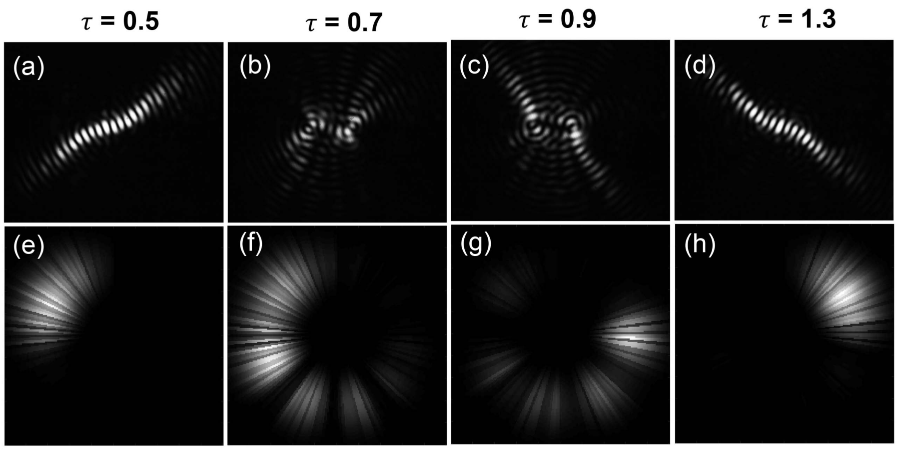

Figure 5. Measurements of a 4-state superposition given by Eq. 11, for $n = 6$ and $q = 30$. Panes (a-d) show the pendulum mode at different scaled times τ. Below the mode images we show the corresponding probability extracted from the images in the Fourier plane and plotted as a function of the pendulum angle θ in polar form.

As time evolves, the mode transforms. This evolution is better understood by observing the measured probability, where it is seen to spread to different angles, showing nodes and antinodes, but with a centroid that seems to mimic the "swinging" of the pendulum to reach the other turning point at $\tau = 1.3$, shown in Figs. 5(d,h). Subsequently at $\tau = 2.1$ the original mode of Figs. 5(a,e) is "almost" recreated. This constitutes a revival with the shortest period. Figures 5(b,f) and (c,g) show examples at intermediate times. The revivals shown in this example evoke other parallels in atomic physics in the revival of atomic Rydberg wavepackets, where the excitation of a superposition of Rydberg states gives rise to an oscillation in the probability mimicking the classic electronic motion along elliptical orbits around the nucleus [28, 29].

In the preceding paragraph we mentioned that at $\tau = 2.1$ the probability after a pendulum "period" is not fully reproduced. This is because it is part of a longer time evolution. A long-term pattern of this case is shown in Fig. 6(a), where the measured probability plotted in "quantum carpet" form [30, 31]. That is, plotting the intensity of the Fourier data, as a function of the pendulum angle along the horizontal scale, displayed parametrically with time along the vertical scale. Each horizontal line of pixels corresponds to a specific time, with each figure containing a compilation of about 800 images taken at different times. Thus, viewed from top to bottom we see the time evolution of the probability for the given superposition. We can first see that at

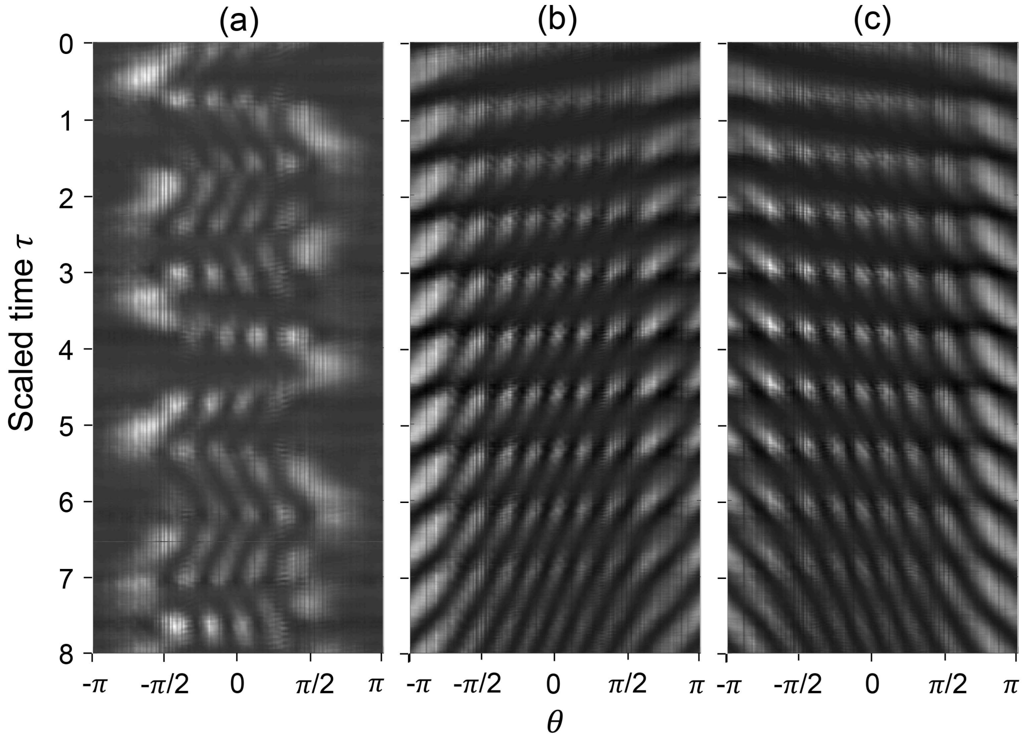

Figure 6. Time evolution of the measured probability of the superposition of 4 states as a function of the pendulum angle θ, plotted parametrically in "carpet" form, where each pixel row corresponds to a distinct time. Case (a) corresponds to $n = 6$ and $a = c = 1/2$ and $b = d = +i/2$ in Eq. 11 for $q = 30$, a librating mode of the pendulum. Cases (b) and (c) correspond to $n = 10$ and $a = c = 1/2$, but with $b = d = +i/2$ for (b) and $b = d = -i/2$ for (c), which are the clockwise and counter-clockwise rotation modes of the pendulum, respectively.

$\tau = 0.5$ the pendulum is at the turning point, as shown above. We can see the one full swing mentioned earlier that ends at $\tau = 2.1$ but a larger revival after a second swing at $\tau = 3.5$. After that we see another single revival at $\tau = 5.2$ followed by not well defined oscillations. The periodicities in the probabilities depend on the range of energy-level separations spanning from 0.09 to 0.36 scaled energy units. These translate in periodicities spanning 2.8 to 11 in scaled time units.

Figure 6(b) shows the measured probability for the case where $n = 10$ also with $a = c = 1/2$ and $b = d = +i/2$ for $q = 30$. This superposition consists of the 4 lowest states above the potential energy barrier. This wavepacket clearly shows the intensity (or equivalently, the probability) moving toward lower values of θ as time increases. This corresponds to a clockwise moving rotor. If we instead specify $b = d = -i/2$ with all else remaining equal, we get the counter-clockwise moving rotor, as shown in Fig. 6(c). This change in handedness of the rotor makes sense because it involves a change of π in the relative phase between the odd and even constituent modes (states).

We have investigated other combinations, such as superpositions of 6 and 8 states, for $q = 50$ and $q = 70$, respectively, and the results are very similar, although the parameter space increases significantly with the possible values of relative amplitude and phase of the initial states. Conversely, one could turn the argument around and engineer superpositions that give rise to specific non-diffractive modal patterns.

5. Discussion and Conclusions

In this article we present the use of modal superpositions of non-diffracting optical beams to analyze a model quantum mechanical system. Current technologies enable us to manipulate the amplitude and phase of the light into specific wave solutions. Nature, acting as an analog computer, does the rest by propagating the light waves. In the particular case of the quantum pendulum we are able to observe stationary states and wavepackets, obtaining a direct display of the predictions of quantum mechanics. The agreement between calculations and measurements is excellent.

An interesting possibility that we are currently investigating involves creating (2+1) dimensional modes by converting the coordinate along the propagation direction (z) proportional to the time evolution of the problem. This can be done by creating superpositions with distinct transverse/longitudinal wave-vectors, which impart a modal relative phase that changes as a function of z [32, 33, 34]. The present study also leads into other new directions. One is the behavior of modes in the high-q limit, which for low-lying states approximate those of the harmonic-oscillator, and to optical modes mimicking optical Gaussian beams, dubbed Gaussian-beam beams [22]. For low q values (e.g., $q = 5$), this system can be used to model the electronic wavefunctions of the transmon system, which consists of 3 unequally spaced states in bound to a harmonic potential [8].

Beyond the intrinsic interest in analyzing quantum systems with light, this system can also be used in a new way in applications such as imaging and particle manipulation [35]. This problem could also be used for educational purposes, because it leads to a textbook-type analysis of a basic quantum mechanical problem, illustrating the interplay between the classical and quantal counterparts.

6. Acknowledgements

This work was funded by NSF grant PHY1506321. We thank M.R. Dennis and S. Chavez-Cerda for helpful discussions.

7. References

[1] Marte M A M and Stenholm S 1997 *Phys. Rev. A* **56** 2940–2953
[2] Condon E U 1928 *Phys. Rev.* **31** 891–894
[3] McLachlan M W 1947 *Theory and Applications of Mathieu Functions* (Oxford University Press)
[4] Friedrich B and Herschbach D R 1991 *Nature* **353** 412–414
[5] Baker G L, Blackburn J A and Smith H J T 2002 *Am. J. Phys.* **70** 525–531
[6] Ayub A, Naseer K, Ali M and Salf F 2009 *J. Russ. Laser Res.* **30** 205–223

[7] Gervin C S, Hoang T M, Land B J, Anquez M, Hamley C D and Chapman M S 2012 *Nat. Comm.* **3** 1169

[8] Koch J, Yu T M, Gambetta J, Houck A A, Schuster D I, Majer J, Blais A, Devoret M H, Girvin S M and Schoelkopf R J 2007 *Phys. Rev. A* **76** 042319

[9] Casati G, Chirikov B V, Israelev F M and Ford J 1979 Stochastic behavior of a quantum pendulum under a periodic perturbation *Stochastic Behavior in Classical and Quantum Hamiltonian Syetems. Lecture Notes in Physics* vol 93 ed Casati G and Ford J (Springer, Berlin, Heidelberg) pp 334–352

[10] Grempel D R, Prange R E and Fishman S 1984 *Phys. Rev. A* **29**(4) 1639–1647

[11] Moore F L, Robinson J C, Bharucha C F, Sundaram B and Raizen M G 1995 *Phys. Rev. Lett.* **75**(25) 4598–4601

[12] Durnin J 1987 *J. Opt. Soc. Am. A* **4** 651–654

[13] Durnin J, Miceli J J and Eberly J H 1987 *Phys. Rev. Lett.* **58**(15) 1499–1501

[14] Gutiérrez-Vega J C, Iturbe-Castillo M D and Chávez-Cerda S 2000 *Opt. Lett.* **25** 1493–1495

[15] Gutiérrez-Vega J C, Iturbe-Castillo M D, Ramírez G A, Tepichín E, Rodríguez-Dagnino R M, Chávez-Cerda S and New G H C 2001 *Opt. Commun.* **195** 35–40

[16] Bandres M A, Gutiérrez-Vega J C and Chávez-Cerda S 2004 *Opt. Lett.* **29** 44–46

[17] López-Mariscal C, Bandres M A, Gutiérrez-Vega J C and Chávez-Cerda S 2005 *Opt. Express* **13** 2364–2369

[18] Berry M V and Balazs N L 1979 *Am. J. Phys.* **47** 264–267

[19] Siviloglou G A, Broky J, Dogariu A and Christodoulides D N 2007 *Phys. Rev. Lett.* **99**(21) 213901

[20] Ring J D, Lindberg J, Mourka A, Mazilu M, Dholakia K and Dennis M R 2012 *Opt. Express* **20** 18955–18966

[21] Nye J F 1999 *Natural Focusing and Fine Structure of Light* (Institute of Physics Publishing)

[22] Dennis M R and Ring J D 2013 *Opt. Lett.* **38** 3325–3328

[23] Strogatz S H 1994 *Nonlinear Dynamics and Chaos: With Applicaitons to Physics, Biology Chemistry and Engineering* (Perseus Books)

[24] Cook G P and Zaidins C S 1986 *Am. J. Phys.* **54** 259–267

[25] Gutiérrez-Vega J C, Rodríguez-Dagnino R M, Meneses-Nava M A and Chávez-Cerda S 2003 *Am. J. Phys.* **71** 233–242

[26] Chávez-Cerda S, Gutiérrez-Vega J C and New G H C 2001 *Opt. Lett.* **26** 1803–1805

[27] Cojocaru E *arXiv:0811.1970v2*

[28] Parker J and Stroud Jr C R 1986 *Phys. Rev. Lett.* **56** 717–719

[29] Yeazell J A and Stroud Jr C R 1991 *Phys. Rev. A* **43** 5153–5156

[30] Großmann F, Rost J M and Schleich W P 1997 *J. Phys. A* **30** L277–L283

[31] Leibscher M and Schmidt B 2009 *Phys. Rev. A* **80** 012510

[32] Schulze C, Roux F S, Dudley A, Rop R, Duparré M and Forbes A 2015 *Phys. Rev. A* **91**(4) 043821

[33] Moreno I, Davis J A, Sánchez-López M M, Badham K and Cottrell D M 2015 *Opt. Lett.* **40** 5451–5454

[34] Holmes B M and Galvez E J 2019 *J. Opt.* **21** 104001

[35] Rubinsztein-Dunlop H, Forbes A, Berry M V, Dennis M R, Andrews D L, Mansuripur M, Denz C, Alpmann C, Banzer P, Bauer T, Karimi E, Marrucci L, Padgett M, Ritsch-Marte M, Litchinitser N M, Bigelow N P, Rosales-Guzmán C, Belmonte A, Torres J P, Neely T W, Baker M, Gordon R, Stilgoe A B, Romero J, White A G, Fickler R, Willner A E, Xie G, McMorran B and Weiner A M 2016 *Journal of Optics* **19** 013001